



HAL
open science

Plasmaspheric Plumes and EMIC Rising Tone Emissions

B. Grison, M. Hanzelka, Hugo Breuillard, F. Darrouzet, O. Santolík, Nicole Cornilleau-Wehrin, I. Dandouras

► **To cite this version:**

B. Grison, M. Hanzelka, Hugo Breuillard, F. Darrouzet, O. Santolík, et al.. Plasmaspheric Plumes and EMIC Rising Tone Emissions. *Journal of Geophysical Research Space Physics*, 2018, 123 (11), pp.9443-9452. 10.1029/2018JA025796 . hal-02408168

HAL Id: hal-02408168

<https://hal.science/hal-02408168>

Submitted on 12 Dec 2019

HAL is a multi-disciplinary open access archive for the deposit and dissemination of scientific research documents, whether they are published or not. The documents may come from teaching and research institutions in France or abroad, or from public or private research centers.

L'archive ouverte pluridisciplinaire **HAL**, est destinée au dépôt et à la diffusion de documents scientifiques de niveau recherche, publiés ou non, émanant des établissements d'enseignement et de recherche français ou étrangers, des laboratoires publics ou privés.

1 Plasmaspheric plumes and EMIC rising tone emissions

2 **B. Grison¹, M. Hanzelka¹, H. Breuillard², F. Darrouzet³, O. Santolík^{1,4}, N.**
3 **Cornilleau-Wehrin² and I. Dandouras⁵**

4 ¹Department of Space Physics, IAP CAS, Boční II 1401, 14131 Prague, Czechia

5 ²Laboratoire de Physique des Plasmas, CNRS/Ecole Polytechnique/Obs. de Paris/UPMC/Univ.
6 Paris-Sud, Palaiseau, France

7 ³Royal Belgian Institute for Space Aeronomy (BIRA-IASB), Brussels, Belgium

8 ⁴Faculty of Mathematics and Physics, Charles University, Prague, Czechia

9 ⁵Institut de Recherche en Astrophysique et Planétologie, University of Toulouse / CNRS / UPS / CNES,
10 Toulouse, France

11 **Key Points:**

- 12 • **Coherent rising tones are found in 20% (6/30) of the plume (and vicin-**
13 **ity) events with EMIC emissions**
- 14 • **EMIC rising tones are observed at magnetic latitudes larger than $\sim 17^\circ$, and up**
15 **to 35°**
- 16 • **Emissions below H^+ gyrofrequency in the vicinity of plasmaspheric plumes are mainly**
17 **broadband**

Corresponding author: Benjamin Grison, grison@ufa.cas.cz

18 **Abstract**

19 Due to its polar orbit Cluster spacecraft crossed plasmaspheric plumes out of the mag-
 20 netic equatorial plane. We study the occurrence of broadband, narrowband and rising
 21 tone emissions in the plume vicinity, below the local **proton** gyrofrequency. Based on
 22 a database of 935 Cluster plumes crossings, reduced to 189 unique plumes, we find that
 23 broadband activity is the most common case. We confirm result from the previous study
 24 showing that plume vicinity is not a preferred place for observing narrowband emissions.
 25 Rising tones are the less frequently observed of these three kind of emissions. Neverthe-
 26 less **ElectroMagnetic Ion Cyclotron (EMIC)** rising tone occurrence rate is high com-
 27 pared to the narrowband one: tones are seen in 6 of **30** plume events (20%) when nar-
 28 rowband emissions are observed. Rising tones are observed at absolute magnetic lati-
 29 tudes larger than $\sim 17^\circ$ and up to 35° . We detail the 16 August 2005 plume crossing when
 30 a rising tone is observed. Results of a ray tracing analysis agree with a tone triggering
 31 process taking place above 15° of magnetic latitude.

32 **1 Introduction**

33 Depending on the background magnetic field (\mathbf{B}_0) intensity and the plasmasphere
 34 extent, local proton gyrofrequency (f_{H^+}) at the Earth's plasmopause typically varies be-
 35 tween 1 and 10 Hz. ElectroMagnetic Ion Cyclotron (EMIC) waves are narrowband emis-
 36 sions observed below f_{H^+} . The free energy for EMIC wave growth mainly results from
 37 proton temperature anisotropy [Kennel and Petschek, 1966] and the wave growth max-
 38 imizes in region of minima of \mathbf{B}_0 and/or of density increase. EMIC emissions are observed
 39 in various part of the magnetosphere including the plasmopause region [e.g., Anderson
 40 *et al.*, 1992; Usanova *et al.*, 2012].

41 When EMIC linear amplification saturates, nonlinear process starts and sub-wavepackets
 42 of increasing frequencies forming rising tones can be observed [Omura *et al.*, 2010]. The
 43 frequency with time dispersion (sweep rate) is a key feature for tone identification in situ
 44 [Pickett *et al.*, 2010]. These emissions are usually referred to as EMIC triggered emis-
 45 sions (referring to generation mechanism) or EMIC rising tones (referring to observa-
 46 tional shape). As the triggering process is not the core of this study, we use EMIC ris-
 47 ing tone name in what follows. Another key parameter for identification is tone emis-
 48 sion coherence level which is higher than the surrounding narrowband EMIC waves [Gri-
 49 son *et al.*, 2013].

50 Plasmaspheric plumes are plasma regions partially detached from plasmasphere con-
 51 secutive to geomagnetic storms or substorms [*Elphic et al.*, 1996, e.g.]. Plasma density
 52 gradients observed in the plumes do not make plumes a preferred region for EMIC wave
 53 observations [*Usanova et al.*, 2013]. Due to the Cluster [*Escoubet et al.*, 2001] polar or-
 54 bit and its perigee inside the plasmasphere, Cluster spacecraft cross plumes off the mag-
 55 netic equatorial plane, where EMIC rising tones have not been reported yet. In this pa-
 56 per we compare the occurrence rate of broadband, narrowband and rising tone emissions,
 57 below f_{H^+} and in the vicinity of plasmaspheric plumes crossed by Cluster.

58 After presenting the instrumentation, the methodology and the occurrence rate of
 59 these three types of emissions (section 2) we detail wave and particle observations and
 60 ray tracing analysis of a plume crossing with rising tone to infer the tone triggering place
 61 (section 3). We discuss (section 4) our results before concluding (section 5).

62 **2 Statistical Study**

63 **2.1 Instrumentation**

64 Each of the four spacecraft of the Cluster mission contains 11 identical instruments
 65 [*Escoubet et al.*, 2001]. The flux gate magnetometer (FGM) data are used for \mathbf{B}_0 mea-
 66 surements and for the magnetic field fluctuation (\mathbf{B}) measurements [*Balogh et al.*, 2001].
 67 In addition to FGM, for the wave analysis we use STAFF experiment waveform data,
 68 hereafter called STAFF-SC [*Cornilleau-Wehrlin et al.*, 2003]. STAFF response is bet-
 69 ter than the FGM one above 1 Hz and vice-versa [*Nykyri et al.*, 2006; *Robert et al.*, 2014].
 70 Both FGM and STAFF-SC instruments can be used for EMIC emission study in the in-
 71 ner magnetosphere region. Electric field fluctuations (\mathbf{E}) are measured in the spacecraft
 72 spin plane by two electric antennas (EFW, *Gustafsson et al.* [2001]). The plasma den-
 73 sity is obtained from the WHISPER relaxation sounder measurements of the plasma fre-
 74 quency [*Décrou et al.*, 2001], when in its range of operation (2-80 kHz), or from the space-
 75 craft potential measured by EFW. Ion energy fluxes are studied with the CIS/HIA ion
 76 energy spectrometer and CIS/CODIF ion mass spectrometer, which provides ion 3D dis-
 77 tributions separately for each of the main species (H^+ , He^+ , He^{2+} , and O^+) [*Rème et al.*,
 78 2001].

79

2.2 Methodology

82

83

84

85

86

87

88

89

90

91

92

93

94

95

We consider a list of 993 plasmaspheric plume crossings by Cluster spacecraft from 1 February 2001 to 1 February 2006 (the 782 cases identified in [Darrouzet *et al.*, 2008], extended to the end of year 2006 [Usanova *et al.*, 2013]). **A plume is identified by a density increase of at least 10 cm^{-3} and a L-width of at least 0.2 Earth radii (R_E) (cf. Darrouzet *et al.* [2008] pp. 2405–2406 for more details).** A single plasmaspheric plume can be crossed in a single hemisphere at least once or in both hemispheres at least twice. There is no case with a spacecraft crossing the magnetic equator inside a plume. There is at most eight crossings of the same plasmaspheric plume: two crossings per spacecraft, one in each hemisphere. The individual 935 plume crossings with available STAFF-SC data can be then reduced to 189 unique plumes. Unique identifiers CXXX and PYYY, where XXX and YYY are 3 digit numbers, are given to each crossing and each plume. Table 1 details the number of crossings per plume. In the most frequent case, the four Cluster spacecraft observe the same plume in a single hemisphere (31 plumes) or in both hemispheres (48 plumes): in the 2001-2006 years period, the spacecraft were nearly always in a close configuration.

80

Table 1. Number of individual crossings of a given plasmaspheric plume by all the Cluster spacecraft.

81

| | 1x | 2x | 3x | 4x | 5x | 6x | 7x | 8x | Total |
|---------------|----|----|----|-----------|----|----|----|-----------|-------|
| 1 hemisphere | 12 | 11 | 13 | 31 | - | - | - | - | 67 |
| 2 hemispheres | - | 12 | 6 | 13 | 9 | 23 | 11 | 48 | 122 |

96

97

98

99

100

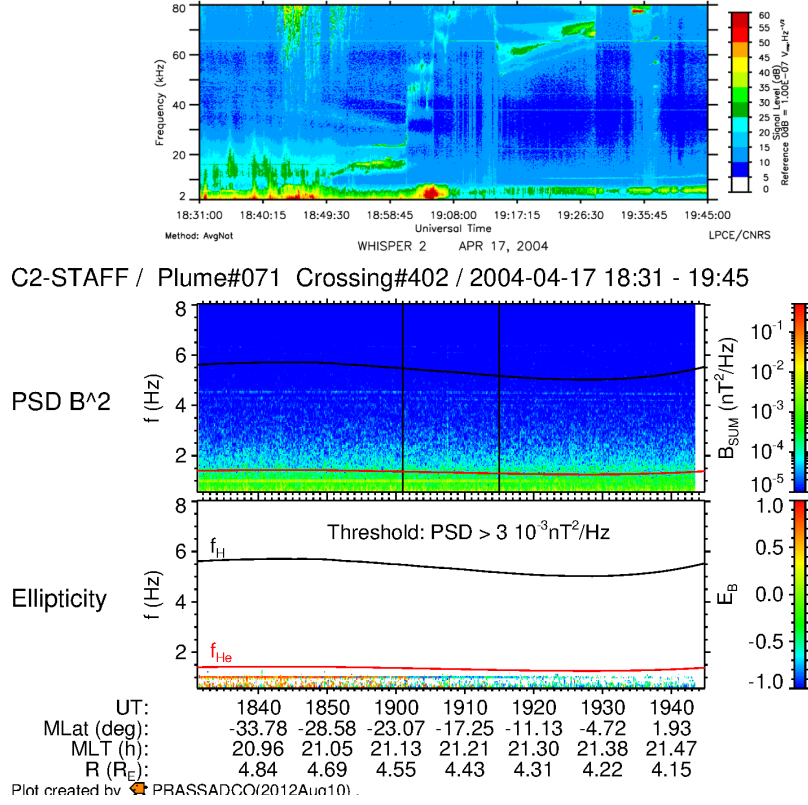
101

102

103

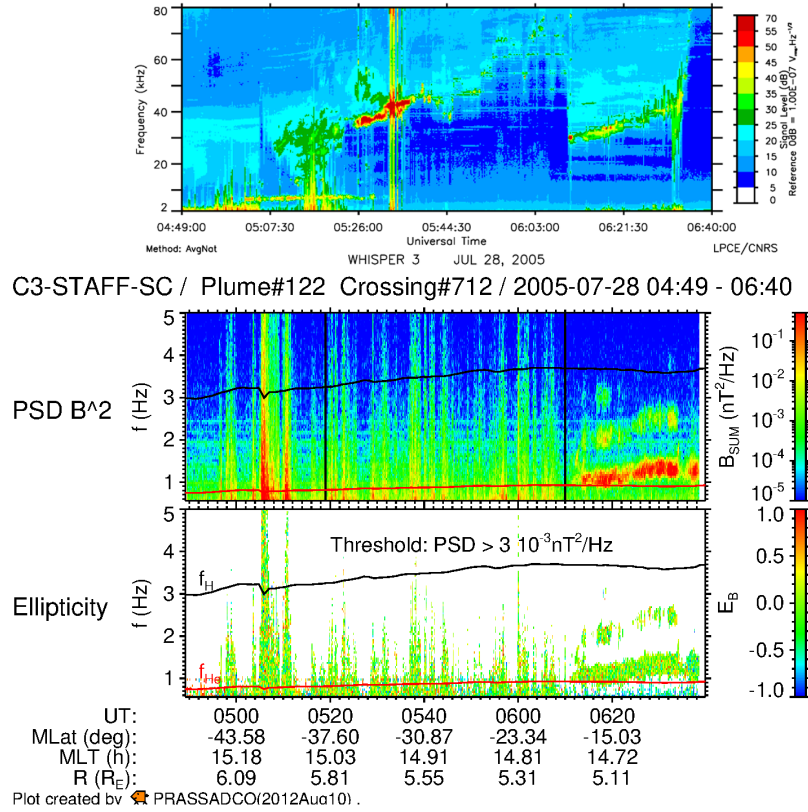
104

For each crossing we report the maximum level of magnetic wave activity (PSD_{max}). Power spectral density (PSD) is computed on 512-point windows (about 20s). There is a 480-point overlap between two consecutive windows. Emissions are classified as, absent or weak (W), for $PSD_{max} < 10^{-3} \text{ nT}^2 \cdot \text{Hz}^{-1}$, and medium (M) for $PSD_{max} \geq 10^{-3} \text{ nT}^2 \cdot \text{Hz}^{-1}$. This is done separately for each type of waves, i.e. broadband, narrowband or rising tone emissions, based on a visual inspection of spectra. Broadband emissions start from the lowest accessible frequency and span over local proton and/or Helium gyrofrequencies, while frequency range of narrowband emissions is limited.



105 **Figure 1. Example of plume crossings (1/2).** Top (WHISPER instrument): **Electric**
 106 **field spectrogram.** Middle (STAFF-SC instrument): total magnetic power spectral
 107 density (PSD) in $\text{nT}^2 \cdot \text{Hz}^{-1}$, two vertical black lines delimit the plume. Bottom (STAFF-SC
 108 **instrument)**: wave ellipticity for emissions with a PSD larger than $10^{-3} \text{ nT}^2 \cdot \text{Hz}^{-1}$. Proton and
 109 He^+ local gyrofrequencies are plotted in black and red solid lines, respectively. **Note that the**
 110 **frequency scale is in kHz in top panel and in Hz in middle and bottom panels.**

112 We show examples of this classification in Figure 1 **and in Figure 2** for two plume
 113 crossings. Top panels present the frequency vs. time diagram (spectrogram) **of the elec-**
 114 **tric field measured by the WHISPER instrument.** The electron plasma fre-
 115 quency (f_{pe}) is identified by intense electrostatic emissions. The plume start
 116 and end times are characterized by abrupt f_{pe} increase and decrease. Mid-
 117 dle panels present the spectrogram of the total magnetic PSD (STAFF-SC in-
 118 strument). Bottom panels present the wave ellipticity with a threshold of $10^{-3} \text{ nT}^2 \cdot \text{Hz}^{-1}$;
 119 it therefore appears only when the wave activity is M. The two vertical lines in the top
 120 panel bound the plume proper. To compare our results with *Usanova et al.* [2013] we
 121 extend the observation time by 30 minutes before and after the plume crossing. On each



111 **Figure 2.** Example of plume crossings (2/2). See Figure 1 for panel description.

122 panel local gyrofrequencies are overplotted in black (f_{H+}) and red (f_{He+}). Universal time
 123 (UT) and spacecraft position, in magnetic latitude (MLAT), magnetic local time (MLT)
 124 and radial distance in Earth radii (R_E), are indicated below the panels.

125 **In Figure 1** (C402, P071) one can see a typical crossing with no wave activity.
 126 The wave activity is set to W for the 3 types of emissions for this crossing. Medium broad-
 127 band emissions are recorded during one (C405, not shown) of the eight P071 plume cross-
 128 ings by the four spacecraft. Plume P071 wave activity is therefore set to W intensity for
 129 the narrowband category and to M intensity for the broadband and overall categories.

130 **In Figure 2** (C712, P122), broadband emissions are observed before and inside
 131 the plume. Narrowband emissions are observed after the plume crossing. For C712, both
 132 broadband and narrowband wave activity are considered in our study as M intensity. Plume
 133 P122 wave activity is also set to M intensity for narrowband and broadband categories.

134 **2.3 Occurrence rate of broadband, narrowband and rising tone emis-**
 135 **sions**

136 **Table 2.** Magnetic power spectral density intensification observed in the vicinity of plasmas-
 137 pheric plumes. W means no or weak activity ($PSD_{max} < 10^{-3} \text{ nT}^2 \cdot \text{Hz}^{-1}$); M means medium
 138 activity ($PSD_{max} \geq 10^{-3} \text{ nT}^2 \cdot \text{Hz}^{-1}$); Tones means rising tones.

| | All | | M-intensity emissions | | |
|-----------------------------|-----|-----|-----------------------|--------|-------|
| | W | M | Broad | Narrow | Tones |
| Plumes | 56 | 133 | 127 | 30 | 6 |
| Plumes (combined crossings) | 231 | 704 | 671 | 175 | 28 |
| M-intensity crossings | - | 444 | 416 | 60 | 9 |
| Crossings / Plumes | 4.1 | 5.3 | 5.3 | 5.8 | 4.7 |
| Hemisphere / Plumes | 1.5 | 1.7 | 1.7 | 1.8 | 1.5 |

139 The results obtained over 189 plumes (and 935 crossings) are summarized in Ta-
 140 ble 2. In 70% of the plume events (133/189) there is a noticeable PSD enhancement. The
 141 average number of individual plume crossings (4.1) is slightly lower in the W category
 142 case compared to the M category (5.3 crossings): the greater the number of spacecraft
 143 crossing of a given plume, the higher the probability to observe waves.

144 Broadband PSD enhancements of M intensity are the most common emissions: they
 145 are observed in two thirds of the plumes (127/189) and in 44 % of the individual cross-
 146 ings (416/935). Such enhancements are present in 62 % of individual crossings (416/671)
 147 in the 127 plumes with broadband emissions. Broadband activity is common in or close
 148 to the plasmaspheric plumes, and it is persistent on the time and/or space scale of the
 149 plume encounter by the Cluster spacecraft.

150 Narrowband emissions are observed close to or in 30 plumes (16 % of the 189 plumes)
 151 and in 6 % of individual crossings (60/935). This is lower than 14 % found by *Usanova*
 152 *et al.* [2013] as discussed in section 4. Narrowband activity is observed in 34 % of indi-
 153 vidual crossings (60/175) in the 30 plumes with narrowband emissions. Narrowband emis-
 154 sions are probably related to more localized processes than the broadband emissions. Nar-
 155 rowband emissions are observed together with broadband activity in six plumes. There
 156 is no correlation between broadband and narrowband activities.

157 For each of the 60 individual crossings with narrowband emissions the presence of
 158 rising tones is investigated. Rising tones are identified by both frequency with time dis-
 159 persion *and* enhanced coherence value. Only tones that can be unambiguously identi-
 160 fied are selected. When observed below 1 Hz, observations are confirmed with FGM data.
 161 Rising tones are observed in only 6 plume events. This number is low with respect to
 162 the total number of plumes (189). Nevertheless one should compare that number with
 163 the 30 plume events where M narrowband activity is noted because narrowband EMIC
 164 waves are seeds for rising tone emissions [*Omura et al.*, 2010]. In 20% of those 30 plumes,
 165 one can also observe rising tones. As large rising tones, clearly identified by eyes, are not
 166 so common (observed first in situ by *Pickett et al.* [2010], a few of them were also reported
 167 by *Grison et al.* [2013]), we consider that **coherent rising tones are a common fea-**
 168 **ture of EMIC emissions in the vicinity of plasmaspheric plumes.**

169 2.4 Rising tone events

170 **Table 3.** Location of rising tone observations (one location per spacecraft per hemisphere).

| Plume # | Crossing # | Date | Time [UT] | SC # | MLAT [°] | MLT [h] | Dist. [R_E] |
|------------|---------------|------------|--------------|---------|-------------|------------|--------------------|
| P038 | C209 | 2002/09/03 | 08:36 | C4 | -35 | 11.7 | 4.6 |
| | C212 | | 10:05 | C4 | 24 | 12.3 | 4.2 |
| P122 | C711 | 2005/07/28 | 02:43 | C2 | -24 | 15.0 | 5.1 |
| | C712 | | 06:12 | C3 | -18 | 14.8 | 5.2 |
| | C715 | | 04:33 | C2 | 27 | 14.4 | 4.7 |
| P126 | C736 | 2005/08/16 | 06:50 | C3 | -23 | 13.5 | 5.3 |
| P140 | C793 | 2006/03/06 | 13:00 | C4 | -17 | 0.5 | 4.8 |
| P163 | C896 | 2006/07/10 | 15:48 | C4 | -17 | 15.9 | 4.6 |
| P169 | C911 | 2006/08/24 | 18:40 | C3 | -26 | 13.6 | 5.2 |

171 Observation places of large rising tones are summarized in Table 3. When more than
 172 one rising tone is observed during a single crossing the given location is the one corre-
 173 sponding to the largest absolute MLAT in each hemisphere. For two plumes the rising
 174 tones were observed in both hemisphere. All events are located at $|\text{MLAT}| > 15^\circ$. Ris-
 175 ing tones are observed up to 35° $|\text{MLAT}|$ (C209). Eight of the nine crossings are located

176 in noon-afternoon sector ([11 h MLT ; 16 h MLT]). Rising tone crossing occurring close
 177 to midnight (C793) is striking as there is a kind of repetition pattern with no EMIC emis-
 178 sions as seed. It presents some similarity with case studied by *Grison et al.* [2016]. Ris-
 179 ing tone observed during crossing C736 will be analyzed in section 3.

180 Besides P140 and P169 that are crossed only once, rising tones are never observed
 181 in every crossings of a plume. The rising tones are observed only in one third (9/28) of
 182 the different crossings of the same plume (see Table 2). This is a highly variable process,
 183 accordingly to the localized phenomenon at the plasmopause noted by *Grison et al.* [2013].
 184 Three of the six plumes, P038, P122, and P126, are crossed in both hemispheres. Ris-
 185 ing tones are observed in each hemisphere in two of these plumes.

186 Rising tones can be observed over a wide range of MLAT (up to 59° for P038) and
 187 over 2.5 h during plume crossings. The low extent in MLT (0.6 h) and radial distance
 188 ($0.4 R_E$) result from the orbit of the Cluster fleet. Cluster perigee and its polar orbit make
 189 the plume encounter rather unlikely close to the magnetic equatorial plane [*Darrouzet*
 190 *et al.*, 2008].

191 **Plasmaspheric plumes occurrence maximizes in the 14-17 MLT sector**
 192 **(see Figure 8 in *Darrouzet et al.* [2008]). Four rising tone events are reported**
 193 **in that sector, four in the 11-14 MLT sector and one in the midnight sector.**
 194 **The noon MLT sector can be thus seen as a preferred sector for rising tone**
 195 **observations. It is worth to notice that the effects of magnetosphere compres-**
 196 **sion are stronger in that sector too.**

197 Based on these results we note that EMIC rising tones, when observed, are com-
 198 mon off the magnetic equatorial plane (above 20° MLAT). Rising tone observations above
 199 20° MLAT are a new result of this study. *Omura et al.* [2010] showed that the equato-
 200 rial plane region was a preferred region for EMIC rising tone triggering process. *Grison*
 201 *et al.* [2016] observed that EMIC tones triggered in the proton branch close to the mag-
 202 netic equatorial plane in the plasmopause density gradient (close to midnight MLT) are
 203 reflected below 15° MLAT.

204 **3 Detailed analysis of a crossing with Rising tone observations (C736)**

205 **3.1 Wave and Particle observations**

213 On 16 August 2005 Cluster-3 crosses a plasmaspheric plume (P126, C736) between
 214 06:00 and 06:41 UT, based on WHISPER plasma frequency data [Darrouzet *et al.*, 2008].
 215 Cluster-3 was the only Cluster spacecraft crossing a plume that day. A large rising tone
 216 (see detailed observations in the following paragraphs) is observed at 06:50 UT just out-
 217 side the plume boundary (vertical black line, panel a). We checked other Cluster space-
 218 craft PSD data: less intense rising tone is seen in Cluster-4 data in the same region about
 219 one minute later. Cluster-4 is ≈ 3000 km away from Cluster-3; both spacecraft follow
 220 almost the same orbit, Cluster-3 moving ahead by about ten minutes.

221 Proton energy-time spectrogram of the particle energy flux (CIS/CODIF instru-
 222 ment) is presented on the top part of Figure 3. Cluster-4/CODIF instrument has the
 223 best sensibility for this event; no such observations are available on Cluster-3. An en-
 224 ergetic ion population (energy above 5 keV) is observed during the 20 minutes window
 225 duration, and is characteristic of the ring current [Dandouras *et al.*, 2018]. The flux in-
 226 tensity of the low-energy (< 100 eV) population intensifies during the event. **It might**
 227 **correspond to tail intensification of the plasmasphere population, marking**
 228 **the plasmasphere approach has discussed hereafter (WHISPER spectrogram**
 229 **on Figure 3).** Between 06:50 and 07:00 (see the previously mentioned lag between Cluster-
 230 3 and Cluster-4), both ion populations are observed, which supports the hypothesis of
 231 a local tone triggering process [Omura *et al.*, 2010]. However the ion temperature anisotropy
 232 remains low during that period. The ratio of the perpendicular to parallel temperature
 233 components is lower than 1.25 (not shown). There is also evidence of a radiation belt
 234 population, starting from 06:40 UT (data not shown).

235 **Middle** part of Figure 3 gathers wave properties obtained from STAFF-SC mea-
 236 surements between 06:35 and 06:55 UT, from top to bottom the total magnetic PSD (a),
 237 coherence in the polarization plane (b), wave vector inclination angle θ_k (c), wave vec-
 238 tor azimuthal angle ϕ_k (d), and ellipticity of polarization (e). These parameters are com-
 239 puted in the frequency domain with the singular value decomposition method [for more
 240 details, see Santolík *et al.*, 2002, 2003]. We could not compute the Poynting flux due to
 241 bad electric field data coverage for that event.

242 A large rising tone is seen at 06:50 UT (Figure 3a). Its foot frequency is just above
 243 f_{He^+} and its frequency extends of about 0.7 Hz, from 1.1 Hz up to 1.8 Hz. The tone sweep
 244 rate is about 10^{-2} Hz·s⁻¹. The coherence of the rising tone (Figure 3b) is remarkably
 245 high as compared to the coherence of emissions of a similar intensity. The wave vector
 246 is more field aligned in the highest frequency part of the tone, where blue is the dom-
 247 inant color, than in the lowest part, where green is the dominant color (Figure 3c and
 248 Table 4). The wave vector is earthward oriented ($\phi_k \approx \pm 180^\circ$, Figure 3d). The tone
 249 ellipticity is clearly left-handed above 1.5 Hz (blue color in Figure 3e). At its foot, EMIC
 250 wave polarization is elliptical and slightly right-handed (yellowish color).

251 **The electric spectrogram (WHISPER instrument) is shown in the bot-**
 252 **tom part of Figure 3. The plasma frequency is plotted in plain white line. Two**
 253 **abrupt decreases are clearly seen (06:37 and 06:41 UT). The second one marks**
 254 **the plume exit. After 06:41, f_{pe} progressively increases, marking the plasma-**
 255 **pause approach.**

256 **Table 4.** Wave vector inclination θ_k of the rising tone (observations).

| Frequency [Hz] | [1.0; 1.2[| [1.2; 1.4[| [1.4; 1.6[| [1.6; 1.8[|
|----------------|------------|------------|------------|------------|
| θ_k [°] | - | 26 | 18 | 10 |

257 Based on the polarization and θ_k angle changes observed as a function of the fre-
 258 quency, we identify the tone mode as the Class III in *Rauch and Roux* [1982] or the mode
 259 4 in *Horne and Thorne* [1993]: it is right-handed polarized below the cross-over frequency
 260 (f_{cr}) and left-handed above it. We recall that f_{cr} is above the cut-off frequency, which
 261 is above f_{He^+} . In the observed frequency range, these waves are mainly field-guided. The
 262 rising tone properties, left-hand polarization, low θ_k , and high coherence level, are mostly
 263 similar to the one observed close to the triggering place [*Omura et al.*, 2010; *Pickett et al.*,
 264 2010; *Grison et al.*, 2013].

265 Assuming that along the field line f_{cr} normalized value ($f_{cr}^* = f_{cr}/f_{H^+}$) remains
 266 the same, the rising tone polarization would be left hand, starting from 1.1 Hz, in a re-
 267 gion where \mathbf{B}_0 intensity is lower than the local one. Trigger should have occurred along
 268 the magnetic field line, considering guided propagation in a dipole magnetic field, some-

269 where between the observation place and the magnetic equatorial plane, where \mathbf{B}_0 in-
 270 tensity along the field line is the lowest.

271 **3.2 Ray tracing analysis**

278 To gain more knowledge concerning the source location and propagation charac-
 279 teristics of the rising tone emission, we perform a ray tracing analysis in cold plasma ap-
 280 proximation. Note that the procedure [*Santolík et al., 2009*] checks for the possible vi-
 281 olation of the WKB approximation at every trajectory point, thus ensuring the valid-
 282 ity of the results. Cold plasma density measurements are not detailed enough in the present
 283 case to reconstruct the density variation in the plasmaspheric plume. We choose to use
 284 a radial density profile based on density measurements and a diffusive equilibrium model.
 285 Additional Gaussian fits to match density measurements are performed. The radial pro-
 286 file is obtained from the spacecraft potential (EFW data) calibrated by WHISPER den-
 287 sity measurements. For the sake of simplicity, Earth’s magnetic field is modeled by a sim-
 288 ple dipole.

289 Initial conditions for the ray tracing analysis are: frequency from 1.0 Hz to 1.9 Hz
 290 with a step of 0.1 Hz, wave normal angle from 10° to 45° with a step of 5° , magnetic lat-
 291 itude $\lambda_m = -23^\circ$, radial distance $R = 5.2 R_E$, and cold plasma populations, includ-
 292 ing heavy ions (5% He^+ and 10% O^+ fractions). Rays are launched from the Cluster-
 293 3 satellite position back to the equator. θ_k and ellipticity are computed along the tra-
 294 jectories. We assume that the polarization reversal seen on panel d of Figure 3 takes place
 295 at the local crossover frequency (≈ 1.0 Hz). Above this frequency, wave vectors with
 296 an initial inclination lower than 30° become parallel before the waves reach the equa-
 297 tor. Changes in heavy ion fractions (up to 10% fraction) lead to similar results. Assum-
 298 ing a parallel generation for the rising tone emission [*Omura et al., 2010*], these waves
 299 should be generated out of the magnetic equatorial plane.

300 We also test emission propagation in a pure electron-proton plasma. Thus the waves
 301 always remain left polarized. Figure 4 shows the latitudinal position of backward traced
 302 waves when the wave normal angle becomes parallel ($\theta_k = 0^\circ$). Only cases when θ_k be-
 303 comes parallel before reaching the magnetic equator are shown. Even in this extreme case
 304 with no heavy ions, none of the rays with initial θ_k below 25° reaches equator before the
 305 wave normal angle drops to 0° .

306 It must be noted that rays with low initial wave normal angles propagated to their
 307 assumed source with almost no dispersion, hinting at possible deficiencies in our mod-
 308 els. We emphasize here that a more complete ray tracing analysis with realistic density,
 309 plasma composition and magnetic field models is left for a further study. Nevertheless
 310 our results, assuming a parallel generation assumption and a non-ducted propagation,
 311 show that the observed rising tone waves are not propagating from the magnetic equa-
 312 torial plane.

313 4 Discussion

314 Our study is based on the list of plasmaspheric plumes and the time intervals (\pm
 315 30 minutes before and after the plume crossing) used in *Usanova et al.* [2013] study. EMIC
 316 emissions are observed in 14% of these time intervals by *Usanova et al.* [2013] and we
 317 observe medium intensity narrowband emissions in 6% of the plume crossings. The PSD
 318 threshold level used in our study (10^{-3} nT²·Hz⁻¹) has a direct impact on the selected
 319 number of events. Other differences between these two studies are different datasets (STAFF
 320 SC data versus FGM data) and methodology (visual inspection versus automatic detec-
 321 tion). Using STAFF-SC data instead of FGM data provides a better coverage of the H⁺-
 322 band and a worse coverage of the He⁺-band. This also contributes to the lower occur-
 323 rence rate found in our study as narrowband EMIC emissions are more frequent in the
 324 He⁺-band than in the H⁺- and O⁺-bands [*Saikin et al.*, 2015]. Conclusions remain un-
 325 changed: plasmaspheric plumes and their vicinity are not a preferred region for obser-
 326 vations of narrowband emissions below local proton gyrofrequency.

327 It is uncommon to observe narrowband emissions and/or rising tones in more than
 328 one third of the crossings of the same plume (60/175 and 9/28 respectively) as can be
 329 seen in Table 2. Narrowband emissions and rising tones are localized in space and time
 330 at lower scales than the characteristic plume scale. Broadband emissions are commonly
 331 observed in the inner magnetosphere region [*Chaston et al.*, 2015]. It is not surprising
 332 to observe them also in the vicinity of plumes.

333 None of the present rising tones (cf. Table 3) are reported in the Cluster survey
 334 of *Grison et al.* [2013]. This survey was performed using a visual inspection of single com-
 335 ponent spectrograms ([http://cluster.lpp.polytechnique.fr/staff/N2nbr/main2018.](http://cluster.lpp.polytechnique.fr/staff/N2nbr/main2018.html)
 336 [html](http://cluster.lpp.polytechnique.fr/staff/N2nbr/main2018.html)). Looking afterwards again at these spectrograms, no rising tones could be visu-

337 ally identified. Reasons are the different spectrogram dynamic scales and the weak PSD
 338 of the rising tone PSD along the component chosen for the spectrogram (along the spin
 339 axis).

340 Considering the degree of polarization and the frequency dispersion, *Nakamura et al.*
 341 [2016] reported a larger occurrence of rising tones (**reported in 30% of the EMIC**
 342 **events**) in the magnetosphere than in the present study. **The equatorial orbit of the**
 343 **THEMIS spacecraft can explain to a large extent these occurrence rate dif-**
 344 **ference as the most favorable local conditions for triggering process are found**
 345 **close to the magnetic equatorial plane. However, this higher occurrence rate**
 346 **might also** be explained by the automatic detection method used in that study which
 347 might be more powerful than visual inspection and by the criterion on the coherence con-
 348 sidered in our study which is more selective than a criterion on the degree of polariza-
 349 tion.

350 An EMIC rising tone generated in the proton branch close to the magnetic equa-
 351 torial plane is reflected toward the magnetic equator at 15° MLAT as reported by *Gri-*
 352 *son et al.* [2016]. We report rising tone observations at absolute magnetic latitudes larger
 353 than 20° . Wave and particle properties, and preliminary ray tracing analysis, indicate
 354 that a propagation of such a rising tone (cf. section 3) from the magnetic equator is un-
 355 likely. We thus believe that rising tones can be triggered at magnetic latitudes above 15° .
 356 **Non-linear process consecutive to saturation of EMIC linear wave growth is**
 357 **more probable in a place where intense EMIC waves are observed.** The trig-
 358 gering region of the rising tones might thus be related to secondary EMIC source region
 359 that was found above 15° MLAT [*Allen et al.*, 2016]. **This region related to parti-**
 360 **cles executing Shabansky orbits is mainly found at higher L-shells (8 to 10),**
 361 **where B_0 is locally depressed, than the rising tone location. However, *Mc-***
 362 ***Collough et al.* [2012] underlined the potential role of plasmaspheric plumes**
 363 **for EMIC growth in this region.**

364 5 Conclusion

365 Starting with 935 plume crossings reduced to 189 unique plumes, we compare the
 366 occurrence rates of broadband, narrowband and rising tones emissions close to plasma-
 367 spheric plumes in the [1-10] Hz frequency range. In time intervals starting 30 minutes

368 before the plume entry and lasting 30 minutes after the plume exit, broadband emissions
369 are the most common emissions (observed in 67 % of the 189 plumes), followed by nar-
370 rowband emissions (in 16 %) and EMIC rising tones (in 3 %).

371 Broadband emissions are not specifically related to plasmaspheric plume as they
372 are commonly observed everywhere in the inner magnetosphere region [*Chaston et al.*,
373 2015]. Based on different dataset and methodology we confirm results of *Usanova et al.*
374 [2013] that the plumes are not a preferred place for narrowband emissions. EMIC ris-
375 ing tones are observed in 20 % of the 30 plumes when narrowband emissions are also ob-
376 served. Tone identification results from a clear frequency dispersion *and* a large coher-
377 ence value. As compared to a few previously reported cases matching these two crite-
378 ria [*Pickett et al.*, 2010; *Grison et al.*, 2013], plumes **and their vicinity appear as a**
379 **common** place for observing EMIC rising tones. We plan to perform in the future an
380 automatic detection of rising tones based on these criteria to confirm that result. The
381 presence of energetic ions associated to a dense cold population and a density gradient
382 can explain the larger occurrence of the non linear stage of EMIC wave growth.

383 Nine new rising tone events are found at absolute magnetic latitudes larger than
384 **17° and for eight of them in the 11-17 MLT sector**. Based on wave properties and
385 preliminary ray tracing analysis performed in a detailed case study, tone propagation from
386 the magnetic equator to the observation place is rather unlikely. We presume that the
387 rising tone generation can take place at magnetic latitudes above 15° as this region is
388 known to be a source region for EMIC waves [*Allen et al.*, 2016]. This might have im-
389 plication for particle precipitations enhanced by large EMIC rising tones [*Shoji and Omura,*
390 2012].

391 **Acknowledgments**

392 **The list of plume is available upon request (contact Fabien.Darrouzet@aeronomie.be)**

393 We acknowledge support of GACR grant No 18-05285S and of the Praemium Academiae
394 Award. Cluster data are publicly available through the Cluster Science Archive (<https://www.cosmos.esa.int/web/csa>). We thank V. Mařatová for her involvement in the
395 preliminary stage of the study.
396

References

397
398
399
400
401
402
403
404
405
406
407
408
409
410
411
412
413
414
415
416
417
418
419
420
421
422
423
424
425
426
427
428

- Allen, R. C., J.-C. Zhang, L. M. Kistler, H. E. Spence, R.-L. Lin, B. Klecker, M. W. Dunlop, M. André, and V. K. Jordanova (2016), A statistical study of EMIC waves observed by Cluster: 2. Associated plasma conditions, *Journal of Geophysical Research (Space Physics)*, *121*, 6458–6479, doi:10.1002/2016JA022541.
- Anderson, B. J., R. E. Erlandson, and L. J. Zanetti (1992), A statistical study of Pc 1-2 magnetic pulsations in the equatorial magnetosphere. I - Equatorial occurrence distributions. II - Wave properties, *Journal of Geophysical Research*, *97*, 3075–3101, doi:10.1029/91JA02706.
- Balogh, A., C. M. Carr, M. H. Acuña, M. W. Dunlop, T. J. Beek, P. Brown, K.-H. Fornacon, E. Georgescu, K.-H. Glassmeier, J. Harris, G. Musmann, T. Oddy, and K. Schwingenschuh (2001), The Cluster magnetic field investigation: overview of in-flight performance and initial results, *Annales Geophysicae*, *19*(10/12), 1207–1217, doi:10.5194/angeo-19-1207-2001.
- Chaston, C. C., J. W. Bonnell, C. A. Kletzing, G. B. Hospodarsky, J. R. Wygant, and C. W. Smith (2015), Broadband low-frequency electromagnetic waves in the inner magnetosphere, *Journal of Geophysical Research (Space Physics)*, *120*, 8603–8615, doi:10.1002/2015JA021690.
- Cornilleau-Wehrin, N., G. Chanteur, S. Perraut, L. Rezeau, P. Robert, A. Roux, C. de Villedary, P. Canu, M. Maksimovic, Y. de Conchy, D. Hubert, C. Lacombe, F. Lefeuvre, M. Parrot, J. L. Pinçon, P. M. E. Décréau, C. C. Harvey, P. Louarn, O. Santolik, H. S. C. Alleyne, M. Roth, T. Chust, O. Le Contel, and S. team (2003), First results obtained by the Cluster STAFF experiment, *Annales Geophysicae*, *21*(2), 437–456, doi:10.5194/angeo-21-437-2003.
- Dandouras, I., S. Rochel-Grimald, C. Vallat, and M. W. Dunlop (2018), *Terrestrial Ring Current: A Review of Cluster Results Based on the Curlometer Technique*, chap. 7, pp. 115–126, American Geophysical Union (AGU), doi: 10.1002/9781119324522.ch7.
- Darrouzet, F., J. De Keyser, P. M. E. Décréau, F. El Lemdani-Mazouz, and X. Vallières (2008), Statistical analysis of plasmaspheric plumes with Cluster/WHISPER observations, *Annales Geophysicae*, *26*(8), 2403–2417, doi: 10.5194/angeo-26-2403-2008.

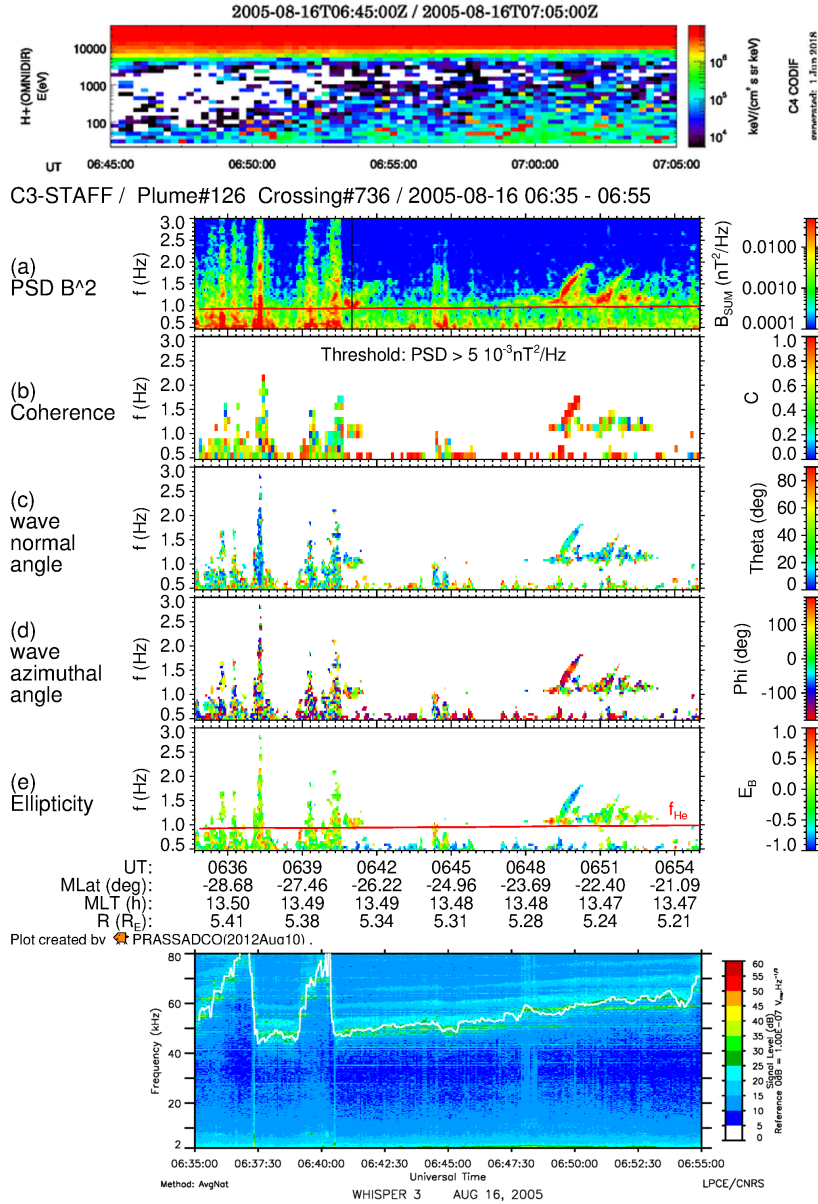
- 429 Décréau, P. M. E., P. Fergeau, V. Krasnoselskikh, E. Le Guirriec, M. Lévêque,
 430 P. Martin, O. Randriamboarison, J. L. Rauch, F. X. Sené, H. C. Séran, J. G.
 431 Trotignon, P. Canu, N. Cornilleau, H. de Féraud, H. Alleyne, K. Yearby, P. B.
 432 Mögensen, G. Gustafsson, M. André, D. C. Gurnett, F. Darrouzet, J. Lemaire,
 433 C. C. Harvey, P. Travnicek, and W. experimenters (Table 1) (2001), Early results
 434 from the WHISPER instrument on Cluster: an overview, *Annales Geophysicae*,
 435 *19*(10/12), 1241–1258, doi:10.5194/angeo-19-1241-2001.
- 436 Elphic, R. C., L. A. Weiss, M. F. Thomsen, D. J. McComas, and M. B. Moldwin
 437 (1996), Evolution of plasmaspheric ions at geosynchronous orbit during times
 438 of high geomagnetic activity, *Geophysical Research Letters*, *23*(16), 2189–2192,
 439 doi:10.1029/96GL02085.
- 440 Escoubet, C. P., M. Fehringer, and M. Goldstein (2001), The Cluster mission, *An-*
 441 *nales Geophysicae*, *19*(10/12), 1197–1200, doi:10.5194/angeo-19-1197-2001.
- 442 Grison, B., O. Santolík, N. Cornilleau-Wehrin, A. Masson, M. J. Engebretson, J. S.
 443 Pickett, Y. Omura, P. Robert, and R. Nomura (2013), EMIC triggered chorus
 444 emissions in Cluster data, *Journal of Geophysical Research (Space Physics)*, *118*,
 445 1159–1169, doi:10.1002/jgra.50178.
- 446 Grison, B., C. P. Escoubet, O. Santolík, N. Cornilleau-Wehrin, and Y. Khotyaintsev
 447 (2014), Wave number determination of Pc 1-2 mantle waves considering He⁺⁺
 448 ions: A Cluster study, *Journal of Geophysical Research (Space Physics)*, *119*,
 449 7601–7614, doi:10.1002/2013JA019719.
- 450 Grison, B., F. Darrouzet, O. Santolk, N. Cornilleau-Wehrin, and A. Masson (2016),
 451 Cluster observations of reflected emic-triggered emission, *Geophysical Research*
 452 *Letters*, *43*(9), 4164–4171, doi:10.1002/2016GL069096.
- 453 Gustafsson, G., M. André, T. Carozzi, A. I. Eriksson, C.-G. Fälthammar, R. Grard,
 454 G. Holmgren, J. A. Holtet, N. Ivchenko, T. Karlsson, Y. Khotyaintsev, S. Klimov,
 455 H. Laakso, P.-A. Lindqvist, B. Lybekk, G. Marklund, F. Mozer, K. Mursula,
 456 A. Pedersen, B. Popielawska, S. Savin, K. Stasiewicz, P. Tanskanen, A. Vaivads,
 457 and J.-E. Wahlund (2001), First results of electric field and density observations
 458 by Cluster EFW based on initial months of operation, *Annales Geophysicae*,
 459 *19*(10/12), 1219–1240, doi:10.5194/angeo-19-1219-2001.
- 460 Horne, R. B., and R. M. Thorne (1993), On the preferred source location for the
 461 convective amplification of ion cyclotron waves, *Journal of Geophysical Research:*

- 462 *Space Physics*, 98(A6), 9233–9247, doi:10.1029/92JA02972.
- 463 Kennel, C. F., and H. E. Petschek (1966), Limit on Stably Trapped Particle Fluxes,
464 *Journal of Geophysical Research*, 71, 1, doi:10.1029/JZ071i001p00001.
- 465 McCollough, J. P., S. R. Elkington, and D. N. Baker (2012), The role of Shabansky
466 orbits in compression-related electromagnetic ion cyclotron wave growth, *Journal*
467 *of Geophysical Research (Space Physics)*, 117, A01208, doi:10.1029/2011JA016948.
- 468 Nakamura, S., Y. Omura, and V. Angelopoulos (2016), A statistical study of emic
469 rising and falling tone emissions observed by themis, *Journal of Geophysical Re-*
470 *search: Space Physics*, 121(9), 8374–8391, doi:10.1002/2016JA022353.
- 471 Nykyri, K., B. Grison, P. J. Cargill, B. Lavraud, E. Lucek, I. Dandouras, A. Balogh,
472 N. Cornilleau-Wehrin, and H. Rème (2006), Origin of the turbulent spectra in
473 the high-altitude cusp: Cluster spacecraft observations, *Ann. Geophys.*, 24(3),
474 1057–1075, doi:10.5194/angeo-24-1057-2006.
- 475 Omura, Y., J. Pickett, B. Grison, O. Santolik, I. Dandouras, M. Engebretson,
476 P. M. E. Décréau, and A. Masson (2010), Theory and observation of electro-
477 magnetic ion cyclotron triggered emissions in the magnetosphere, *Journal of Geo-*
478 *physical Research (Space Physics)*, 115(A14), A07234, doi:10.1029/2010JA015300.
- 479 Pickett, J. S., B. Grison, Y. Omura, M. J. Engebretson, I. Dandouras, A. Mas-
480 son, M. L. Adrian, O. Santolík, P. M. E. Décréau, N. Cornilleau-Wehrin, and
481 D. Constantinescu (2010), Cluster observations of EMIC triggered emissions in
482 association with Pc1 waves near Earth’s plasmopause, *Geophys. Res. Lett.*, 37,
483 L09104, doi:10.1029/2010GL042648.
- 484 Rauch, J. L., and A. Roux (1982), Ray tracing of ulf waves in a multicomponent
485 magnetospheric plasma: Consequences for the generation mechanism of ion cy-
486 clotron waves, *Journal of Geophysical Research: Space Physics*, 87(A10), 8191–
487 8198, doi:10.1029/JA087iA10p08191.
- 488 Rème, H., C. Aoustin, J. M. Bosqued, I. Dandouras, B. Lavraud, J. A. Sauvaud,
489 A. Barthe, J. Bouyssou, T. Camus, O. Coeur-Joly, A. Cros, J. Cuvilo, F. Ducay,
490 Y. Garbarowitz, J. L. Medale, E. Penou, H. Perrier, D. Romefort, J. Rouzaud,
491 C. Vallat, D. Alcaydé, C. Jacquy, C. Mazelle, C. d’Uston, E. Möbius, L. M.
492 Kistler, K. Crocker, M. Granoff, C. Moukikis, M. Popecki, M. Vosbury, B. Klecker,
493 D. Hovestadt, H. Kucharek, E. Kuenneth, G. Paschmann, M. Scholer, N. Scokopke,
494 E. Seidenschwang, C. W. Carlson, D. W. Curtis, C. Ingraham, R. P. Lin, J. P.

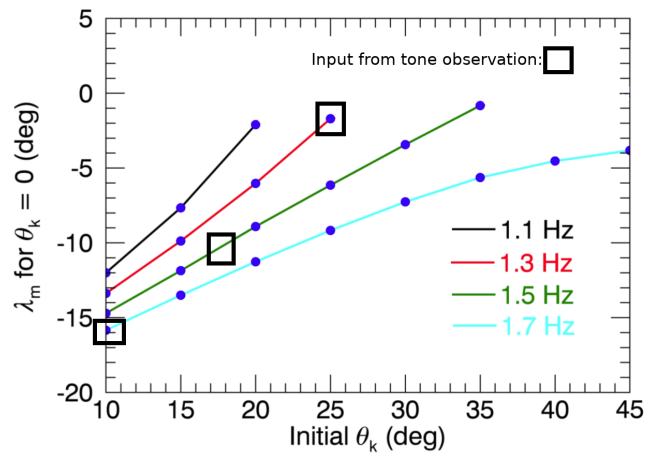
- 495 McFadden, G. K. Parks, T. Phan, V. Formisano, E. Amata, M. B. Bavassano-
 496 Cattaneo, P. Baldetti, R. Bruno, G. Chionchio, A. Di Lellis, M. F. Marcucci,
 497 G. Pallochia, A. Korth, P. W. Daly, B. Graeve, H. Rosenbauer, V. Vasyliunas,
 498 M. McCarthy, M. Wilber, L. Eliasson, R. Lundin, S. Olsen, E. G. Shelley, S. Fuse-
 499 lier, A. G. Ghielmetti, W. Lennartsson, C. P. Escoubet, H. Balsiger, R. Friedel, J.-
 500 B. Cao, R. A. Kovrazhkin, I. Papamastorakis, R. Pellat, J. Scudder, and B. Son-
 501 nerup (2001), First multispacecraft ion measurements in and near the Earth's
 502 magnetosphere with the identical Cluster ion spectrometry (CIS) experiment,
 503 *Ann. Geophys.*, *19*(10/12), 1303–1354, doi:10.5194/angeo-19-1303-2001.
- 504 Robert, P., N. Cornilleau-Wehrin, R. Piberne, Y. de Conchy, C. Lacombe,
 505 V. Bouzid, B. Grison, D. Alison, and P. Canu (2014), CLUSTER–STAFF search
 506 coil magnetometer calibration– comparisons with FGM, *Geoscientific Instrumen-*
 507 *tation, Methods and Data Systems*, *3*(2), 153–177, doi:10.5194/gi-3-153-2014.
- 508 Saikin, A. A., J. Zhang, R. C. Allen, C. W. Smith, L. M. Kistler, H. E. Spence,
 509 R. B. Torbert, C. A. Kletzing, and V. K. Jordanova (2015), The occurrence and
 510 wave properties of H⁺-, He⁺-, and O⁺-band EMIC waves observed by the Van
 511 Allen Probes, *Journal of Geophysical Research: Space Physics*, *120*(9), 7477–7492,
 512 doi:10.1002/2015JA021358.
- 513 Santolík, O., J. S. Pickett, D. A. Gurnett, and L. R. O. Storey (2002), Magnetic
 514 component of narrowband ion cyclotron waves in the auroral zone, *Journal of*
 515 *Geophysical Research (Space Physics)*, *107*, 1444, doi:10.1029/2001JA000146.
- 516 Santolík, O., M. Parrot, and F. Lefeuvre (2003), Singular value decomposition meth-
 517 ods for wave propagation analysis, *Radio Sci.*, *38*(1), doi:10.1029/2000RS002523,
 518 1010.
- 519 Santolík, O., M. Parrot, U. S. Inan, D. Burešová, D. A. Gurnett, and J. Chum
 520 (2009), Propagation of unducted whistlers from their source lightning: A
 521 case study, *Journal of Geophysical Research: Space Physics*, *114*(A3), doi:
 522 10.1029/2008JA013776.
- 523 Shoji, M., and Y. Omura (2012), Precipitation of Highly Energetic Protons by He-
 524 lium 1 Branch Electromagnetic Ion Cyclotron Triggered Emissions, *Journal of*
 525 *Geophysical Research*, *117*, A12210, doi:10.1029/2012JA017933.
- 526 Usanova, M. E., I. R. Mann, J. Bortnik, L. Shao, and V. Angelopoulos (2012),
 527 THEMIS Observations of EMIC Wave Occurrence: Dependence on AE, SYMH,

528 and Solar Wind Dynamic Pressure, *Journal of Geophysical Research*, *117*, A10218,
529 doi:10.1029/2012JA018049.

530 Usanova, M. E., F. Darrouzet, I. R. Mann, and J. Bortnik (2013), Statistical analy-
531 sis of EMIC waves in plasmaspheric plumes from Cluster observations, *Journal of*
532 *Geophysical Research: Space Physics*, *118*(8), 4946–4951, doi:10.1002/jgra.50464.



206 **Figure 3.** Wave and particle observations (16 August 2005). Top: Proton energy-time spec-
 207 trogram, in particle energy flux units (all directions, Cluster-4/CODIF data). **Middle:** Wave
 208 properties (Cluster-3/STAFF-SC data). Large rising tone is seen at 06:50 UT. Spacecraft exits
 209 the plume at 06:41 (vertical black line, panel a). The 10 minute lag between wave and particle
 210 windows takes into account Cluster-3/Cluster-4 separation. Bottom: **Electric field spectro-**
 211 **gram (WHISPER instrument).** Plasma frequency is overplotted in white. STAFF-
 212 **SC and WHISPER plots have the same timescale.**



272 **Figure 4.** Results of ray tracing analysis (backward propagation) with negligible population
 273 of He^+ and O^+ . Magnetic latitude (λ_m) at which the wave vector becomes parallel (or reaches
 274 the magnetic equator) is plotted with respect to the initial wave normal angle (θ_k) of the wave
 275 at $\lambda_m = -23^\circ$. Blue dots show that the waves always stay left polarized. Only some of the lower
 276 frequency waves with very oblique initial wave normal angles reach the equator before becoming
 277 parallel. Results for the observational values are indicated by squares.